

Surface Quality Control of p-type Silicon Chip during Edge Insulation with Wire Electric Discharge Machining

Hsin-Min Lee,¹ Ta-Jen Peng,² Tzung-Ming Chen,^{3*} and Kang-Feng Peng⁴

¹Department of Mechanical and Computer-Aided Engineering, Army Academy R. O. C.
No. 750, Longdong Rd., Zhongli Dist., Taoyuan City 320316, Taiwan

²Department of Intelligent Automation Engineering, National Chin-Yi University of Technology
No. 57, Sec. 2, Zhongshan Rd., Taiping Dist., Taichung City 411030, Taiwan

³Department of Industrial Education and Technology, National Changhua University of Education
No. 2, Shi-Da Rd., Changhua City 500208, Taiwan

⁴Department of Mechanical Engineering, National Central University
No. 300, Zhongda Rd., Zhongli Dist., Taoyuan City 320317, Taiwan

(Received August 5, 2023; accepted October 26, 2023)

Keywords: energy saving, WEDM, surface roughness, crystal edge insulation, polycrystalline silicon

Solar energy is one of the most widely used green energy sources, but the consumption of chemicals during the manufacturing of solar panels lowers the environmental value of this source. Therefore, in this study, we apply wire electrical discharge machining to the edge insulation process of solar cell chips to avoid the disadvantages of using chemical edge insulation and reduce the cost of waste liquid disposal. In addition, process parameters, such as servo voltage, feed rate, machining depth, discharge gap, droplet flow rate, and the concentration of abrasive powder added, are investigated to improve the surface roughness of specimens, as well as to remove the phosphorus layer and minimize cracks on the specimen surface. The experimental results indicate that the surface roughness of silicon chips can be reduced from 0.614 to 0.365 μm using deionized water with a droplet flow rate of 12 cc/min at the servo voltage of 30 V, which resulted in a 40% improvement in the surface roughness of silicon chips. The addition of 0.6 g/l SiC to deionized water further reduced the surface roughness to 0.304 μm , which represented a 10% improvement over the value achieved with pure deionized water. This means that the need for a chemical post-treatment process can be reduced while maintaining the surface quality of the specimen and ensuring environmental protection. At the same time, the removal of the phosphorus layer and cracks in one single process pass demonstrates that wire electric discharge machining can be used efficiently for wafer edge insulation.

1. Introduction

Solar energy is one of the main alternative and green energy sources from the perspective of mitigating the global energy crisis because of its wide geographical applicability and modularity⁽¹⁾ and the fact that solar energy systems can be installed on rooftops, by the roadside, at sea, and even in the desert. In addition, solar panels have low maintenance threshold, are easy

*Corresponding author: e-mail: tmchen@cc.ncue.edu.tw
<https://doi.org/10.18494/SAM4692>

to install, and have good scalability and long service life. Therefore, it is worthwhile to conduct an in-depth exploration of the materials, manufacturing processes, and other technologies related to solar panels. The production of solar cell chips from silicon wafers is among the mainstream processes nowadays. Silicon is the second most abundant element on Earth. It is nontoxic, stable in oxide form, and insoluble in water. Depending on its crystallization arrangement, silicon can be classified as monocrystalline, polycrystalline, and amorphous.^(2–4) The photovoltaic conversion efficiency of polycrystalline silicon has increased from 14–15% in the early days to more than 17%, whereas that of monocrystalline silicon has increased from 17% to more than 20%. The larger the frontal area of the chip that is exposed to light, the higher is its efficiency. In terms of the resource consumption costs of the existing chemical edge insulator process,^(5–7) the costs of HF, HNO₃, and waste liquid treatment are US\$1.14/l, US\$0.67/l, and US\$0.2/kg, respectively. Accordingly, for a production capacity of 500000 wafers per day, the annual costs of HF, HNO₃, and waste liquid treatment would be approximately US\$210000, US\$400000, and US\$140000, respectively. The total cost would exceed US\$750000 per year. In addition, the costs of postprocessing procedures required to address the surface damage caused by laser cutting must be considered. Therefore, in this study, we investigate the use of wire electric discharge machining (WEDM) in the edge insulation process of solar cell silicon chips to reduce the production cost of solar cells through process selection and parameter control, as well as to improve process yields, while considering environmental protection.

The process parameters of WEDM directly affect the surface roughness and mechanical properties of the resulting solar cells. In 2015, Sharma *et al.*⁽⁸⁾ implemented WEDM on Inconel 706, and their experimental results proved that process parameters, such as servo voltage, pulse processing, and rest time, significantly affect various process outcomes, such as material removal rate, surface roughness, the surface morphology of recast layers, microhardness, microstructure, and metallurgical changes. In 2016, Ayesta *et al.*⁽⁹⁾ implemented WEDM on Inconel 718, an aerospace material, and the results of various experiments, such as material metallographic analysis, residual stress analysis, and cross-sectional and axial fatigue tests, indicated significant increases in the fatigue resistance and service life of the material. In 2017, Baburaja *et al.*⁽¹⁰⁾ applied WEDM to Hastelloy C-276 and aluminum in an experiment where they varied several process parameters, such as the pulse machining time, line tension, feed rate, and delay time. The results of this experiment highlighted the considerable contributions of these parameters to the surface roughness of the resulting samples and the erosion rate of the WEDM process. In 2017, Goswami and Kuma⁽¹¹⁾ utilized Taguchi's method to design an experimental table for the WEDM of nickel alloys and predicted the material removal rate, surface roughness, and electrode wear rate. The experimental results agreed well with the predicted values, and they indicated a high level of improvement in the surface quality of a structure. In 2019, Selvakumar *et al.*⁽¹²⁾ used open-circuit voltage and line tension, among others, as the control parameters of WEDM to achieve the desired surface roughness of a specimen. Their results indicated that just one processing run was effective for achieving the desired surface roughness, and multiple processing runs adversely affected the specimen's accuracy. In 2021, Sagbas *et al.*⁽¹³⁾ developed a neural network model to predict the surface roughness of WEDM-processed specimens. Their results indicated that open-circuit voltage and feed rate were the main parameters affecting the surface quality of the specimens.

The materials and specifications of the electrodes used in WEDM directly affect the quality of processed surfaces. In 2007, Chak and Rao⁽¹⁴⁾ coated diamond particles on the surface of electrodes used for the electrochemical discharge machining (ECDM) of ceramic materials. Their experimental results indicated that the depth and accuracy of machining achieved using diamond-coated electrodes were superior to those achieved using electrodes without diamond coating. In 2016, Saha and Mondal⁽¹⁵⁾ utilized a zinc-coated brass wire as an electrode in the WEDM of nanostructured hard-faced materials, and their experimental results highlighted pulse time as one of the important parameters affecting material processing. Moreover, the zinc-coated brass wire electrode was able to improve several machining qualities, such as material removal rate, machining time, and surface roughness, relative to those achieved with a naked brass wire electrode. In 2017, Kuo *et al.*⁽¹⁶⁾ included auxiliary electrodes in experiments involving the WEDM of tool steel and aluminum. Their experimental results demonstrated that the surface properties of the resulting specimens, such as surface roughness, surface alloying, and microhardness, improved. In 2023, Dhale and Deshmukh⁽¹⁷⁾ compared the effects of three electrode wire diameters, namely, 150, 200, and 250 μm , on the quality of WEDM processing. According to their results, electrode wires with smaller diameters relatively reduce the variation in the microhardness of the processed surfaces owing to improve debris removal and positively affect the surface quality of the resulting specimens owing to reduce surface damage.

The benefits of incorporating additional grinding particles into the electrolyte have been studied. In 2007, Han *et al.*⁽¹⁸⁾ added graphite powder to the electrolyte and used the conductive property of graphite powder to disperse the energy of ECDM for improving the accuracy of the machined surface. According to the experimental results, the addition of 1 wt% graphite reduced the surface roughness from Ra 4.86 μm to Ra 1.44 μm after machining. In 2019, Sivaprakasam *et al.*⁽¹⁹⁾ conducted 27 experiments based on a full factorial design by varying each of the three parameters, namely, voltage, capacitance, and powder concentration. The experimental results indicated that the addition of 0.5 g/l graphite nanopowder to the electrolyte significantly improved the morphology of the machined surface, and the roughness of the machined surface decreased from Ra 0.830 μm to Ra 0.418 μm . Moreover, other studies^(20–24) have demonstrated that the addition of powder can effectively improve the surface roughness of machined specimens.

On the basis of this literature review, we consider that it is worthwhile to explore the use of relevant WEDM process parameters, electrode selection, and abrasive particle addition to enhance the surface quality of silicon chips in the edge insulation process.

2. Experimental Methods

2.1 Equipment

The experimental equipment is based on an engraving EDM method with an additional micro-EDM system for the edge processing of silicon chips. The system consists of a WEDM grinding and cutting mechanism, a three-axis (X , Y , θ) microfeed rotary mechanism added to the Z -axis, and a specimen clamping mechanism. The DC power required for the experiment is

supplied using an external power supply, and an oscilloscope is used to observe changes in current. A peristaltic pump is employed to provide a steady electrolyte flow to ensure silicon chip removal. In addition, a camera is used to observe the machining situation and confirm the accuracy of the machining position.

2.2 Parameters

The servo voltage ranged from 30 to 50 V, the droplet flow rate ranged from 7.2 to 14.4 cc/min, the machining depth ranged from 30 to 50 μm , and the feed rate ranged from 600 to 1000 $\mu\text{m}/\text{min}$. Before machining, Y-axis and Z-axis zeroings were performed, and then the Y-axis discharging gap was set to 30 and 60 μm . Deionized water was used as the electrolyte, and SiC powder was added to it in concentrations of 0.2, 0.4, and 0.6 g/l. The machining parameters are listed in Table 1.

2.3 Materials

In this experiment, a p-type polysilicon specimen measuring $6 \times 4 \times 0.2 \text{ mm}^3$ was used for edge processing. The properties of the chip are listed in Table 2. The surface of the wafer was roughened using an etching machine; then, the wafer was processed using a diffusion machine to infiltrate phosphorus on its surface; finally, the wafer was cut using a laser cutting machine, and silicon chips were removed from it. In this study, a $\text{Ø}150 \mu\text{m}$ brass wire was employed as the WEDM electrode, and its mechanical properties and electrical conductivity were suitable for high-temperature environments, as summarized in Table 3.

Because polycrystalline silicon is a semiconductor and the electrolyte is deionized water, it is necessary to use an auxiliary electrode to ensure that these two electrodes can form a loop easily during processing. The auxiliary electrode must have low activity as well as good chemical

Table 1
Process parameters.

Electrolyte droplet flow rate (cc/min)	7.2, 9.6, 12, 14.4, 16.8
Working voltage (V)	30, 35, 40, 45, 50
Discharge gap (μm)	30, 60
Machining depth (μm)	30, 50
Machining speed ($\mu\text{m}/\text{min}$)	600, 700, 800, 900, 1000
Silicon carbide concentration (g/l)	0.2, 0.4, 0.6

Table 2
Properties of silicon chip.

Atomic weight	28.08
Density (g/cm^3)	2.33
Crystal structure	Diamond
Melting point ($^{\circ}\text{C}$)	1414
Boiling point ($^{\circ}\text{C}$)	2900
Thermal conductivity ($\text{W}/\text{m}\cdot\text{k}$)	149
Electrical resistivity ($\Omega\cdot\text{cm}$)	1000

Table 3
Properties of brass wire.

Diameter (μm)	150
Yield strength (MPa)	75
Tensile strength (MPa)	300
Elastic modulus (GPa)	97
Electrical resistivity ($\Omega\cdot\text{cm}$)	8×10^{-8}
Melting point ($^{\circ}\text{C}$)	905

stability and conductivity to ensure that it facilitates electrolysis, which affects the electrolyte quality. Therefore, an auxiliary graphite electrode is used herein. The properties of graphite are summarized in Table 4. Moreover, the material properties of the electrolyte are summarized in Table 5, and the relevant components and specifications of the SiC powder added to the electrolyte are listed in Table 6.

3. Results and Discussion

The surface roughness of the specimen immediately after laser cutting and before the WEDM process was $0.614 \mu\text{m}$, as measured using a three-dimensional (3D) profilometer and illustrated in Fig. 1(a). The edge of the specimen had many cracks, as observed by a scanning electron microscopy (SEM) and illustrated in Fig. 1(b). The thickness of the phosphorus diffusion layer in the specimen was $0.2 \mu\text{m}$, and the phosphorus content of the specimen before processing was

Table 4
Characteristics of graphite (auxiliary electrode).

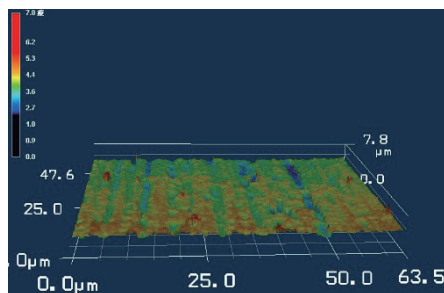
Density (g/cm^3)	1.89
Young's modulus (kg/mm^2)	1200
Flexural strength (kg/mm^2)	4.9
Electrical resistivity ($\text{M}\Omega\cdot\text{cm}$)	950
Coefficient of thermal expansion ($10^{-6}/^\circ\text{C}$)	4.8

Table 5
Properties and specifications of deionized water.

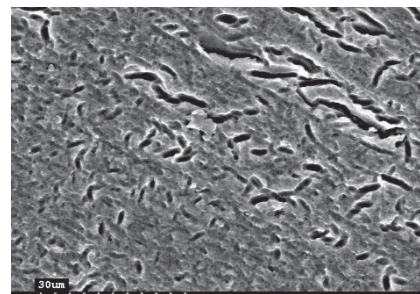
Chemical	H_2O
Atomic weight	18.015
Density (kg/m^3)	1000
Specific heat ($\text{cal}/\text{g}^\circ\text{C}$)	0.999
Melting point ($^\circ\text{C}$)	0
Boiling point ($^\circ\text{C}$)	100
Viscosity ($\text{Pa}\cdot\text{s}$, 20°C)	0.001
Specific resistance ($\text{M}\Omega\cdot\text{cm}$, 20°C)	23.8
Conductivity ($\mu\text{s}/\text{cm}$)	2

Table 6
Properties and specifications of SiC powder.

Mesh	#8000
Maximum grain size (μm)	6
Average grain size (μm)	0.9–1.5
Molar mass (g/mol)	40.09
Density (g/cm^3)	3.22
Melting point ($^\circ\text{C}$)	2730



(a)



(b)

Fig. 1. (Color online) Quantification and qualitative characterization of specimen surfaces after laser cutting and before WEDM process. (a) The surface roughness is Ra $0.614 \mu\text{m}$. (b) Large number of cracks on specimen surface.

10.84% according to the results of X-ray photoelectron spectroscopy (XPS) analysis. In this study, six process parameters, namely, droplet flow rate, discharge gap, servo voltage, feed rate, machining depth, and the concentration of abrasive powder added, were considered to reduce the surface roughness to less than $0.4 \mu\text{m}$ by WEDM, as well as to remove the phosphorus diffusion layer completely to ensure insulation.

3.1 Droplet flow and feed rates

A peristaltic pump was used to control the flow rate of electrolyte droplets in the WEDM process, ensure inter-electrode insulation and impact pressure generation, and achieve specimen cooling and chip removal. According to the experimental results, debris was not accumulated on the machined surface when the droplet flow rate ranged from 12 to 16.8 cc/min. The discharge frequency cycle was stable, and the discharge spark was uniform. Therefore, a surface roughness lower than $Ra\ 0.614 \mu\text{m}$ could be achieved. The same situation was observed for the feed rates of 600 and 1000 $\mu\text{m}/\text{min}$, as depicted in Fig. 2.

Among them, the discharge pits formed on the machined surface when the droplet flow rate was 12 cc/min were significantly smaller and had better shapes, and the measured surface roughness was $Ra\ 0.40 \mu\text{m}$, as illustrated in Fig. 3(a). However, when the droplet flow rates were 7.2 and 9.2 cc/min, it was difficult to remove debris, resulting in a reduction in the number of discharges and the generation of uneven and concentrated discharge spots. In addition, the generated debris remaining between the two processing surfaces in conjunction with the brass wire could likely squeeze the specimen. This could alter the width of the discharge gap and cause the discharge spark to become unstable, resulting in the generation of coarse discharge pits and the poor appearance of the finished surface. After processing, the resulting surface roughness was worse than $Ra\ 0.614 \mu\text{m}$. For example, the measured surface roughness corresponding to the feed rate of 600 $\mu\text{m}/\text{min}$ and the electrolyte flow rate of 7.2 cc/min was $Ra\ 0.77\mu\text{m}$, as illustrated in Fig. 3(b).

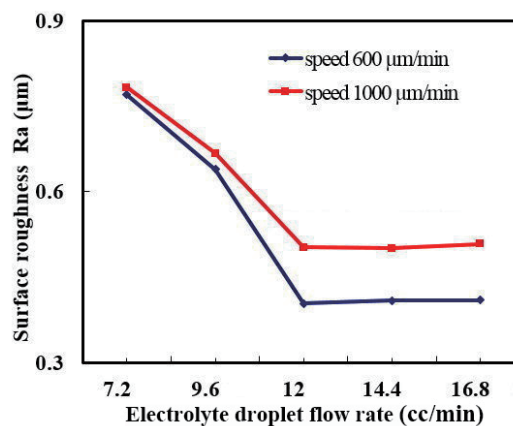


Fig. 2. (Color online) Effects of different feed and electrolyte droplet flow rates on surface roughness.

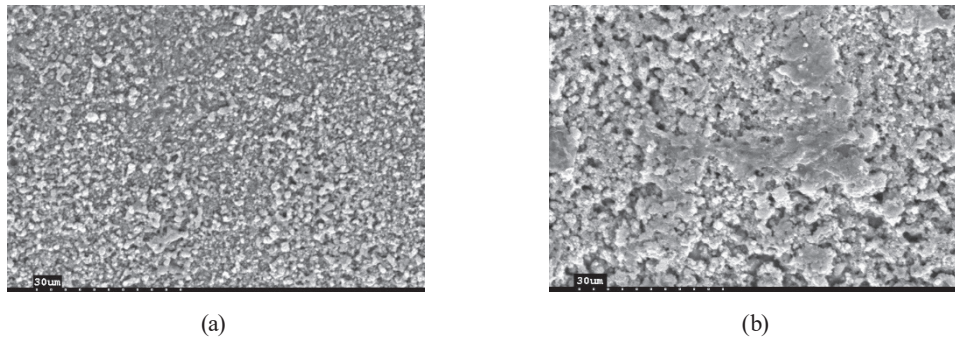


Fig. 3. SEM images of processed surface using electrolyte flow rates of (a) 12 and (b) 7.2 cc/min.

3.2 Machining depth and servo voltage

In this section, the specimen surface quality achievable with servo voltages of 30–50 V and two processing depths of 50 and 30 μm is discussed. The experimental results indicate that under the same servo voltage, processing depth is inversely proportional to surface roughness, that is, the surface roughness achieved with the processing depth of 30 μm is better than that achieved with 50 μm . Moreover, under the same processing depth, servo voltage is inversely proportional to surface roughness. Further analysis indicated that by using combinations of processing depths of 50 and 30 μm with servo voltages of 30–40 V, surface roughnesses lower than Ra 0.614 μm can be achieved, and the corresponding measurement data are presented in Fig. 4.

Increasing the machining depth relatively increases the wire tension, and the higher the wire tension, the higher the allowable feeding rate. However, the high amount of heat generated by the discharge under high wire tension will expand and soften the brass wire. For example, the combination of a processing depth of 50 μm and a processing voltage of 50 V easily induces wire breakage. In addition, although higher servo voltages can increase machining efficiency, they damage the machined surface more severely, as can be inferred from the SEM surface morphology images presented in Fig. 5(a). This was because as the servo voltage increased, the discharge energy density increased, and the size of the hot melting zone increased. Consequently, the melting condition around the material was uneven and out of control, and the measured surface roughness increased to Ra 1.64 μm . By contrast, surface quality values of Ra 0.614 μm or lower can be obtained with the machining depths of 50 and 30 μm at servo voltages lower than 40 V. Moreover, according to the results of texture analysis, the surface quality achieved with the machining depth of 50 μm and the servo voltage of 30 V was higher than that achieved with the machining depth of 50 μm and the servo voltage of 40 V, as can be inferred from the SEM images presented in Figs. 5(b) and 5(c). The brass wire did not swell or soften in this appropriate servo voltage range. At this time, the bubbles formed owing to the combined effect of electrolyte flow and brass wire electrode movement can merge rapidly to form a complete insulating gas film. Subsequently, the insulation film breaks down to form a plasma channel, resulting in a stable and uniform discharge frequency and discharge sparks.

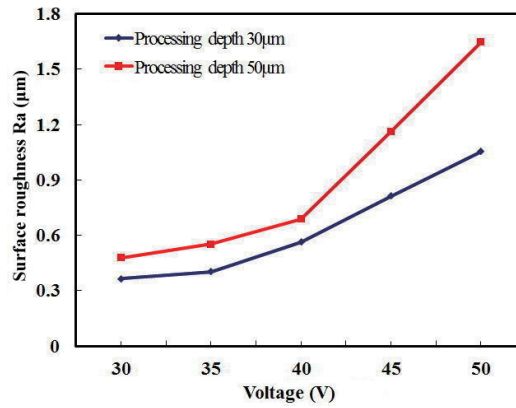


Fig. 4. (Color online) Effects of different machining depths and servo voltages on surface roughness.

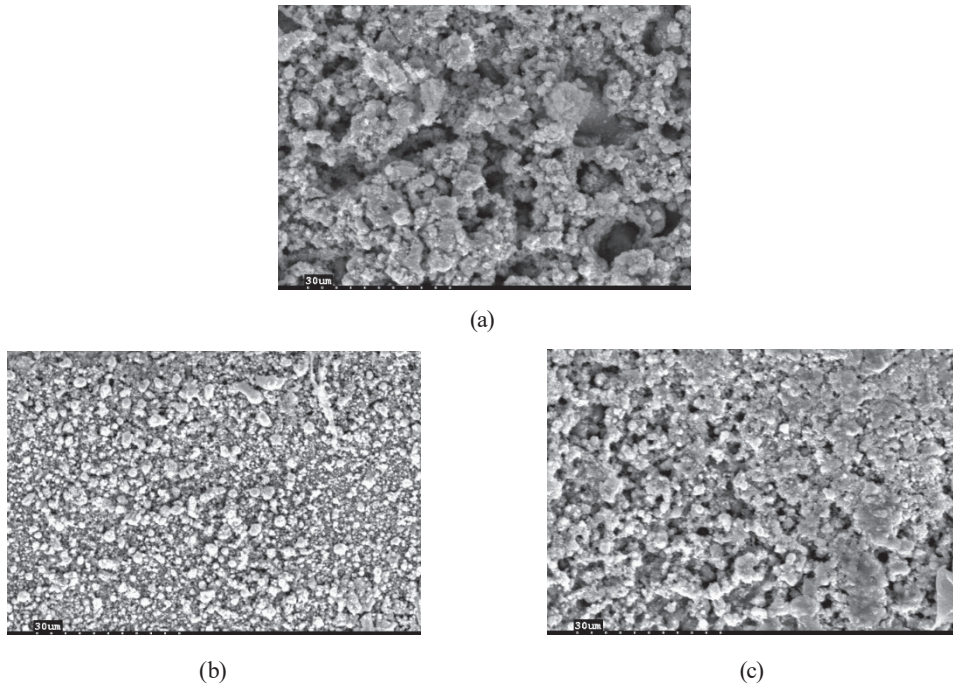


Fig. 5. SEM images of surface processed using combinations of machining depth of 50 μm and different servo voltages: (a) 50 μm–50 V, (b) 50 μm–30 V, and (c) 50 μm–40 V.

3.3 Discharge gap and servo voltage

By using deionized water as the electrolyte, the effects of servo voltages of 30–50 V with discharge gaps of 30 and 60 μm on the surface roughness of processed specimens were investigated under three fixed parameters, namely, an electrolyte flow rate of 12 cc/min, a feed rate of 600 μm/min, and a machining depth of 30 μm. The experimental results indicated that the combinations of discharge gaps of 30 and 60 μm with servo voltages of 30–40 V were able to control the surface roughness to less than Ra 0.614 μm, and the measured data are presented in

Fig. 6. Further analysis indicated that at the same servo voltages, discharge gap was inversely proportional to surface roughness, because the larger the discharge gap, the smaller the likelihood of energy concentration in the discharge column. For example, at the servo voltage of 50 V and the discharge gap of 60 μm , SEM surface morphology observations revealed that the machined surface was severely damaged, as shown in Fig. 7(a). For the same discharge gap, servo voltage was inversely proportional to surface roughness; for instance, the surface quality achieved with the discharge gap of 60 μm and the servo voltage of 30 V was superior to that achieved with the discharge gap of 60 μm and the servo voltage of 40 V, as illustrated in the SEM images in Figs. 7(b) and 7(c).

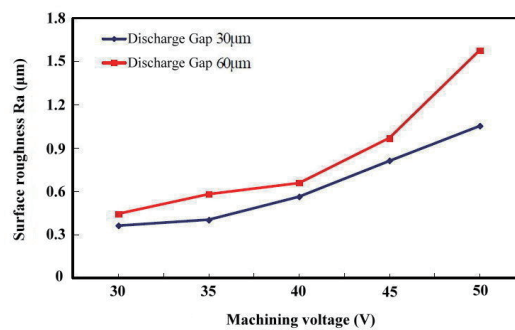


Fig. 6. (Color online) Effects of different servo voltages and discharge gaps on surface roughness.

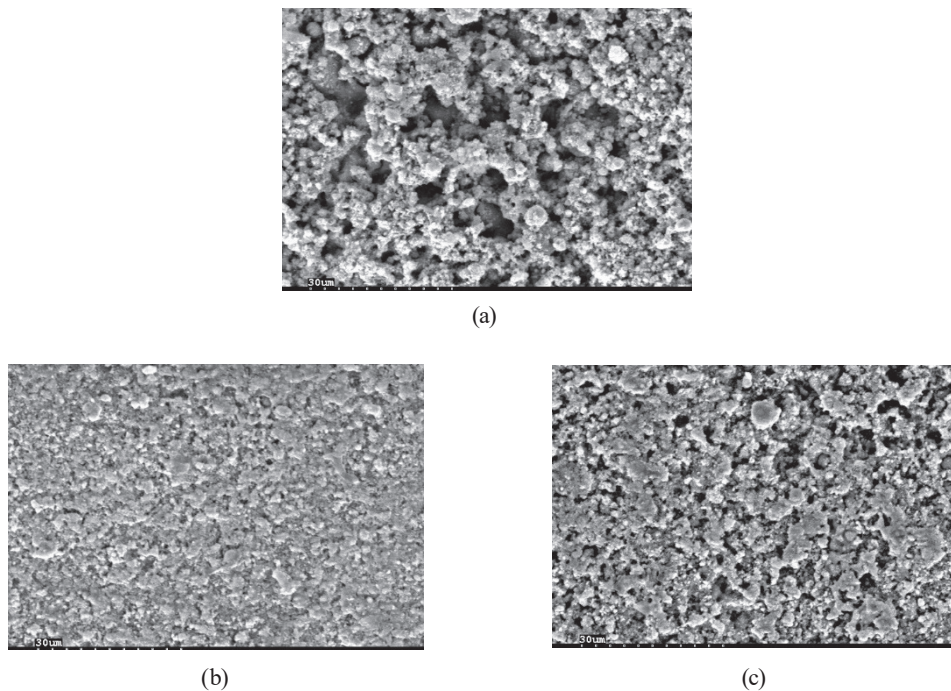


Fig. 7. SEM images of surface processed with combinations of discharge gap of 60 μm and different servo voltages: (a) 60 μm –50 V, (b) 60 μm –30 V, and (c) 60 μm –40 V.

3.4 Feed rate and servo voltage

Basic experiments confirmed that at feed rates of less than 600 $\mu\text{m}/\text{min}$, although the discharge can be stabilized, the discharge sparks tend to be concentrated and cause wire breakage. By contrast, at feed rates of 1000 $\mu\text{m}/\text{min}$ or higher, although wire breakage does not occur easily at higher machining rates, complete material removal in a single pass is not possible, which increases the machining process cost. Therefore, in this section, the effects of five feed rates, namely, 600, 700, 800, 900, and 1000 $\mu\text{m}/\text{min}$, on the surface roughness of processed specimens are investigated under the following machining conditions: a fixed machining depth of 30 μm , a discharge gap of 30 μm , an electrolyte flow rate of 12 cc/min, and servo voltages of 30–50 V. The experimental results indicate that the surface roughness can be controlled to less than Ra 0.614 μm with servo voltages of 30–40 V in the feed rate range of 600–800 $\mu\text{m}/\text{min}$. Under the same servo voltage, feed rate is inversely proportional to surface roughness. Under the same feed rate, servo voltage is inversely proportional to surface roughness, and the measured data are presented in Fig. 8. Further analysis indicates that from the perspective of effectively improving the surface quality of the specimen, the feed rates of 900 and 1000 $\mu\text{m}/\text{min}$ can be used only with the servo voltage of 30 V. This is because higher feed rates lead to the uneven distribution of discharge sparks, and when the discharge is incomplete, the electrode has already moved to a new position and restarted the discharge mechanism, resulting in different discharge start and stoppage conditions. Because the formation of the aforementioned insulating film cannot be effectively controlled, the discharge sparks cannot be concentrated, which results in poor surface roughness after machining. Therefore, the higher the feed rate, the smaller the range of servo voltages that can be used.

SEM images of the surface morphologies generated at the feed rates of 600 and 1000 $\mu\text{m}/\text{min}$ in the servo voltage range of 30–50V are presented in Fig. 9. When the servo voltage is 30 V and the feed rate is 600 $\mu\text{m}/\text{min}$, the electrolyte can remove the chips stably. As a result, the discharge sparks are distributed evenly and form a stable discharge state, which can effectively reflect the surface topography, as illustrated in Fig. 9(a). At the servo voltage of 40 V, clear discharge pits are formed on the machined surface, as illustrated in Fig. 9(b). At 50 V, irregular shapes and coarser discharge pits are formed on the machined surface, as shown in Fig. 9(c).

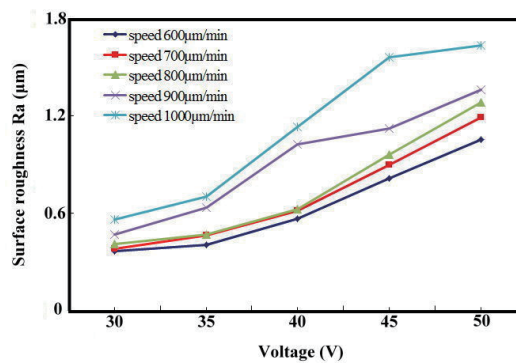


Fig. 8. (Color online) Effects of different servo voltages and feed rates on surface roughness.

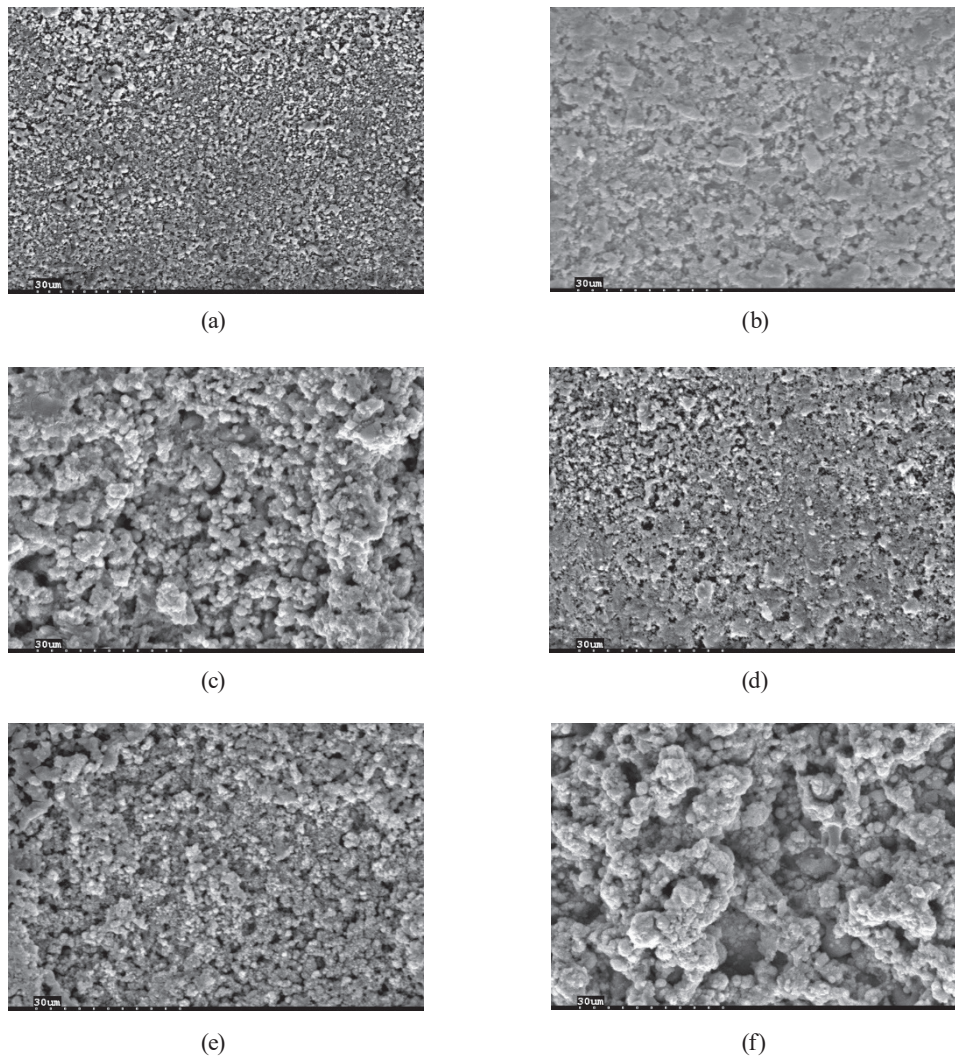


Fig. 9. SEM images of surface processed using different feed rates and servo voltages: (a) 600 $\mu\text{m}/\text{min}$ –30 V, (b) 600 $\mu\text{m}/\text{min}$ –40 V, (c) 600 $\mu\text{m}/\text{min}$ –50 V, (d) 1000 $\mu\text{m}/\text{min}$ –30 V, (e) 1000 $\mu\text{m}/\text{min}$ –40 V, and (f) 1000 $\mu\text{m}/\text{min}$ –50 V.

According to the above analysis, as the servo voltage increases, the discharge energy increases. This results in the formation of more intense discharge sparks, intensifies the effect of high-temperature corrosion on the material, and deteriorates the surface roughness. The same trend is observed at the feed rate of 1000 $\mu\text{m}/\text{min}$, as shown in Figs. 9(d)–9(f).

3.5 Additive concentration and servo voltage

To confirm the possibility of further improving the surface quality of the specimen, we investigated the effect of adding SiC abrasive particles at concentrations of 0.2–0.6 g/l to the electrolyte (deionized water) and setting the servo voltage to 30–50 V. The experimental results indicate that under the same servo voltage, the SiC powder concentration is proportional to the

surface quality. Various combinations of SiC powder concentrations of 0.2–0.6 g/l and servo voltages of 30–40 V can control the surface roughness to less than Ra 0.614 μm , and the measured data are presented in Fig. 10.

Further analysis indicated that the SiC powder concentration had a minor effect on the surface roughness of the specimen at lower voltages. The measured surface roughness was Ra 0.365 μm under the servo voltage of 30 V, but it was Ra 0.36 μm under the same servo voltage after the addition of 0.2 g/l SiC powder, which is almost identical to that when no powder was added. However, when the SiC powder concentration was 0.6 g/l, the surface roughness was Ra 0.304 μm , which represents a significant improvement of 17% compared with the value of Ra 0.365 μm achieved without adding any powder to deionized water.

The higher the servo voltage, the more effective the addition of SiC in improving the surface roughness. Although the surface roughness was negatively affected by the larger discharge pits generated at 50 V, the addition of 0.6 g/l SiC powder reduced the surface roughness from Ra 1.054 μm to Ra 0.77 μm , which represents an improvement of 27%, as shown in Figs. 11(a)–11(c). Similarly, the SEM images indicate that under the servo voltage of 30 V, an increase in SiC powder concentration can effectively counteract the surface damage caused by the discharge pits on the specimen surface, that is, the grinding effect of 0.6 g/l is superior to that of 0.2 g/l, as shown in Figs. 11(d)–11(f).

3.6 Dephosphorization process

On the basis of the parameters presented in the previous sections, it can be determined that with the combination of an electrolyte droplet flow rate of 12 cc/min, a discharge gap of 30 μm , servo voltage of 30 V, a feed rate of 600 $\mu\text{m}/\text{min}$, and a machining depth of 30 μm , the surface roughness of Ra 0.365 μm can be achieved using deionized water as the electrolyte. This value is 40% higher than that of the unprocessed specimen, and the phosphorus layer can be eliminated to realize edge insulation. The phosphorus content in percentage terms, as measured with XPS, is close to 0%, which is consistent with the surface roughness. In addition, to improve the surface flatness of the specimen, deionized water can be supplemented with 0.6 g/l SiC, and the surface roughness of the specimen can be further reduced to 0.304 μm , which is 10% better than

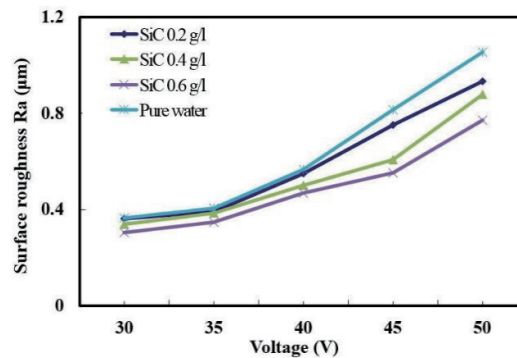


Fig. 10. (Color online) Effects of different servo voltages and SiC powder concentrations on surface roughness.

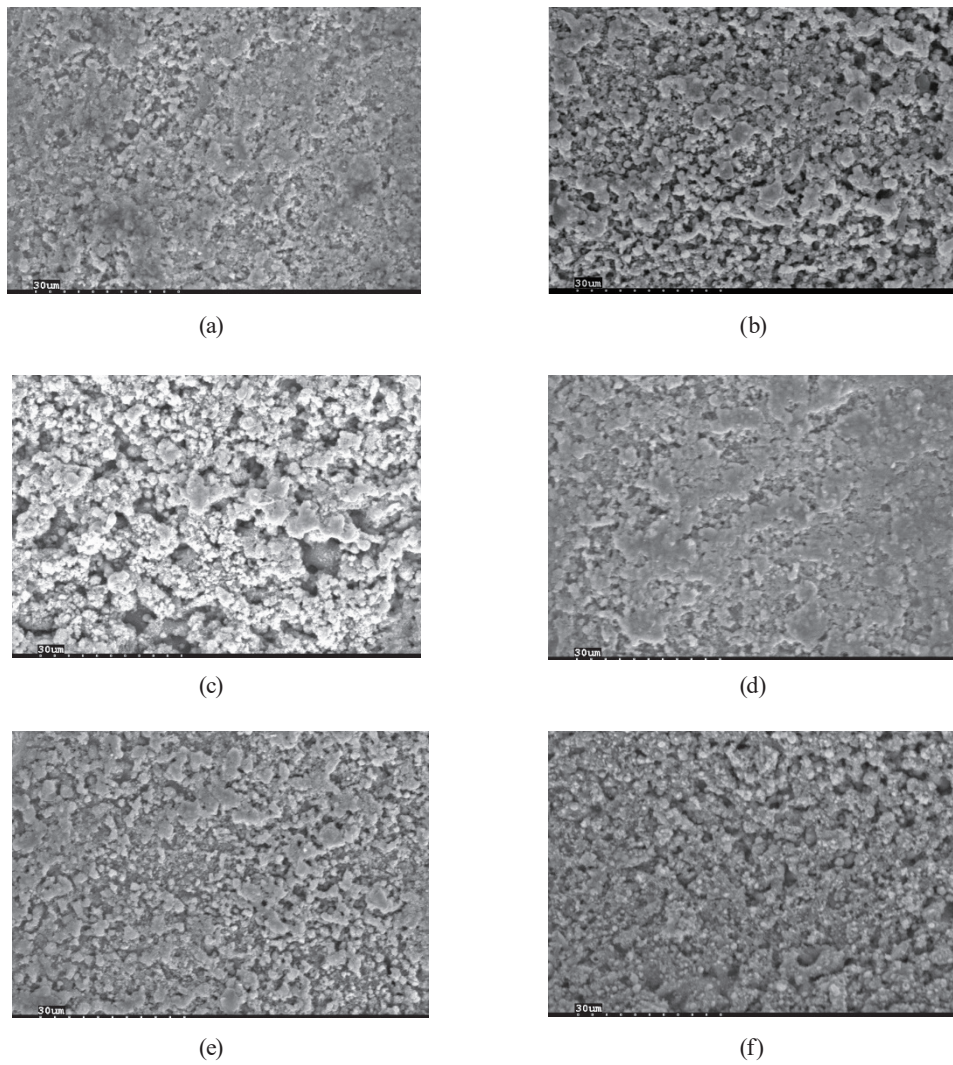


Fig. 11. SEM images of surface processed with different SiC powder concentrations and servo voltages: (a) 0.2 g/l–30 V, (b) 0.2 g/l–40 V, (c) 0.2 g/l–50 V, (d) 0.6 g/l–30 V, (e) 0.6 g/l–40 V, and (f) 0.6 g/l–50 V.

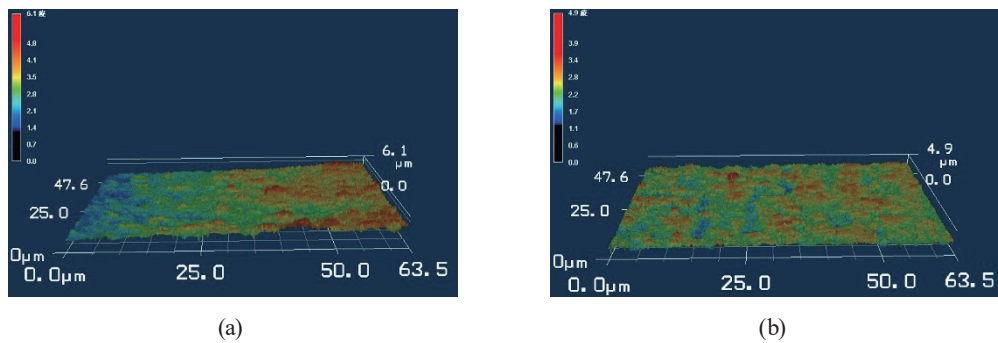


Fig. 12. (Color online) Surface profiles obtained with different SiC powder contents in the electrolyte: (a) pure deionized water and (b) deionized water containing 0.6 g/l SiC powder.

the result obtained without adding SiC powder. The surface of the specimen before WEDM was wavy, as measured with a 3D surface profiler and depicted in Fig. 1(a); the corresponding SEM image is presented in Fig. 1(b). The 3D surface machined without SiC addition has a flat profile, as shown in Fig. 12(a), and the corresponding SEM image is shown in Fig. 9(a), which has been significantly improved. After the addition of 0.6 g/l SiC powder, the 3D surface profile was flatter, as shown in Fig. 12(b), and the corresponding SEM image is shown in Fig. 11(d).

4. Conclusions

To sum up, in the case of the dephosphorization edging process with WEDM, it was confirmed that a sustainable technology is needed for optimization, and a set of suitable parameters was determined to obtain the desired product quality. The main conclusions are summarized as follows:

1. The thickness of the phosphorus diffusion layer before processing was 0.2 μm and the surface roughness was Ra 0.614 μm . The layer was effectively removed, and the surface roughness was improved to Ra 0.365 μm with a single pass of WEDM processing. The surface quality was improved by 40%.
2. In the servo voltage range of 30–40 V, when using deionized water as the electrolyte, the feed rate of 600 $\mu\text{m}/\text{min}$ provided a better surface roughness than that provided by the feed rate of 1000 $\mu\text{m}/\text{min}$. Therefore, the appropriate feed rate can effectively control the formation of the insulating gas film and avoid the concentration of electric sparks, which can improve the surface roughness of machined specimens.
3. When the electrolyte droplet flow rate was equal to or higher than 12 cc/min, the surface roughness was maintained at Ra 0.35–0.4 μm , and it improved with the addition of SiC powder. The surface roughness obtained by adding 0.6 g/l SiC powder to the electrolyte at the lower servo voltages of 30–40 V was more than 10% higher than that achieved by processing with deionized water alone. The surface roughness improvement reached 25% when the servo voltage was 50 V, which proved that the addition of SiC powder to the electrolyte had an abrasive effect on the machined surface.
4. We confirmed that the WEDM process can resolve the issues of HF and HNO₃ consumption, as well as reduce the treatment cost of waste chemicals. In addition, the use of deionized water and auxiliary electrodes to form a discharge circuit can avoid the need for the recycling and treatment of the oily electrolyte. This is in line with the direction of sustainability, and the results can be used as a reference for subsequent research and practice in the manufacturing industry.

Although the process discussed in this study corresponds to sustainability, there remain a few issues that should be optimized continuously. The selection of different types of electrolyte and the analysis of discharge stability and performance are preliminary steps to refine the surface quality of products in the future. Electrolyte recycling is an issue that must be handled under the premise of environmental protection.

References

- 1 A. E. Karaca and I. Dincer: Energy Convers. Manag. **280** (2023) 1. <https://doi.org/10.1016/j.enconman.2023.116808>
- 2 T. Shahabi, H. Heidarzadeh, and H. Bahador: Opt. Commun. **544** (2023) 1. <https://doi.org/10.1016/j.optcom.2023.129623>
- 3 C. Zhu, Y. Seguchi, M. Okugawa, C. Guo, and Y. Koizumi: Materialia **27** (2023) 1. <https://doi.org/10.1016/j.mtla.2023.101702>
- 4 M. L. Addonizio and A. Antonaia: Vacuum **215** (2023) 1. <https://doi.org/10.1016/j.vacuum.2023.112284>
- 5 H. L. Hao, S. H. Zhong, X. Zhang, and W. Z. Shen: Appl. Surf. Sci. **311** (2014) 870. <https://doi.org/10.1016/j.apsusc.2014.05.078>
- 6 J. Arumughan, T. Pernau, A. Hauser, and I. Melnyk: Sol. Energy Mater. Sol. Cells **87** (2005) 705. <https://doi.org/10.1016/j.solmat.2004.06.018>
- 7 A. Otaegi, V. Fano, M. A. Rasool, J. R. Gutiérrez, and J. C. Jimeno: Sol. Energy **155** (2017) 847. <https://doi.org/10.1016/j.solener.2017.07.030>
- 8 P. Sharma, D. Chakradhar, and S. Narendranath: Mater. Des. **88** (2015) 558. <https://doi.org/10.1016/j.matdes.2015.09.036>
- 9 I. Ayesta, B. Izquierdo, O. Flaño, J. A. Sánchez, J. Albizuri, and R. Avilés: Int. J. Fatigue **92** (2016) 220. <https://doi.org/10.1016/j.ijfatigue.2016.07.011>
- 10 K. Baburaja, K. V. Subbaiah, T. Vanaja, and N. N. Ramesh: Mater. Today: Proc. **4** (2017) 1013. <https://doi.org/10.1016/j.matpr.2017.01.114>
- 11 A. Goswami and J. Kuma: Eng. Sci. Technol. Int. J. **20** (2017) 175. <https://doi.org/10.1016/j.jestch.2016.09.016>
- 12 G. Selvakumar, V. Balasubramanian, S. Vijayan, and N. Lenin: Mater. Test. **61** (2019) 901. <https://doi.org/10.3139/120.111400>
- 13 A. Sagbas, F. Gürtuna, and U. Polat: Mater. Test. **63** (2021) 386. <https://doi.org/10.1515/mt-2020-0057>
- 14 S. K. Chak and P. V. Rao: Int. J. Mach. Tools Manuf. **47** (2007) 2061. <https://doi.org/10.1016/j.ijmactools.2007.05.009>
- 15 A. Saha and S. C. Mondal: Measurement **94** (2016) 46. <https://doi.org/10.1016/j.measurement.2016.07.087>
- 16 C. Kuo, H. Kao, and H. Wang: J. Mater. Process. Technol. **244** (2017) 136. <https://doi.org/10.1016/j.jmatprotec.2017.01.025>
- 17 S. R. Dhale and B. B. Deshmukh: Mater. Today: Proc. **72** (2023) 896. <https://doi.org/10.1016/j.matpr.2022.09.088>
- 18 M. Han, B. Min, and S. Lee: J. Mater. Process. Technol. **191** (2007) 224. <https://doi.org/10.1016/j.jmatprotec.2007.03.004>
- 19 P. Sivaprakasam, P. Hariharan, and S. Gowri: Measurement **147** (2019) 1. <https://doi.org/10.1016/j.measurement.2019.07.072>
- 20 A. Kimura, Y. Okamoto, A. Okada, J. Ohya, and T. Yamauchi: Procedia CIRP **6** (2013) 232. <https://doi.org/10.1016/j.procir.2013.03.052>
- 21 P. Sivaprakasam and P. Hariharan: Mater. Today: Proc. **38** (2021) 494. <https://doi.org/10.1016/j.matpr.2020.02.329>
- 22 H. Chow, B. Yan, F. Huang, and J. Hung: J. Mater. Process. Technol. **101** (2000) 95. [https://doi.org/10.1016/S0924-0136\(99\)00458-6](https://doi.org/10.1016/S0924-0136(99)00458-6)
- 23 A. Schubert, V. D. Bui, I. Schaarschmidt, T. Berger, and A. Martin: Procedia CIRP **113** (2022) 100. <https://doi.org/10.1016/j.procir.2022.09.134>
- 24 K. Ishfaq and M. U. Waseem: CIRP J. Manuf. Sci. Technol. **41** (2023) 196. <https://doi.org/10.1016/j.cirpj.2022.11.018>